Controlling the Transport Properties of Gold Nanotubule Membranes Using Chemisorbed Thiols

Sang Bok Lee and Charles R. Martin*

Department of Chemistry and Center for Chemical Research at the Bio/Nano Interface, University of Florida, Gainesville, Florida 32611

Received January 31, 2001. Revised Manuscript Received April 10, 2001

We have developed a new class of synthetic membranes that consist of a porous polymeric support that contains an ensemble of gold nanotubules that span the complete thickness of the support membrane. The support is a commercially available microporous polycarbonate filter with cylindrical nanoscopic pores. The gold nanotubules are prepared via electroless deposition of Au onto the pore walls; that is, the pores act as templates for the nanotubules. We have shown that by controlling the Au deposition time, Au nanotubules that have effective inside diameters of molecular dimensions (<1 nm) can be prepared. Hence, these membranes are a new class of molecular sieves. In addition, because the tubules are composed of gold, well-known Au-thiol chemistry can be used to change the chemical environment within the tubules. This paper reviews recent research on using chemisorbed thiols to control the transport properties of Au nanotubule membranes. The use of both electrical neutral thiols to introduce chemical-transport selectivity and charged thiols to introduce ion-transport selectivity is reviewed.

I. Introduction

We have been investigating a general method for preparing nanomaterials called template synthesis.[1−3] This method entails synthesis or deposition of the desired material within the cylindrical and monodisperse pores of a microporous membrane or other solid. We have used microporous polycarbonate filters, prepared via the track-etch method,[4] and microporous aluminas, prepared electrochemically from Al foil,[5] as our template materials. Cylindrical nanostructures with monodisperse diameters and lengths are obtained, and depending on the membrane and synthetic method used, these may be solid nanowires or hollow nanotubules. We, and others, have used this method to prepare nanoparticles composed of metals,[5−15] polymers,[16−19] semiconductors,[20,21] carbons,[22−24] and Li^+ intercalation materials.[25−27] It is also possible to prepare composite nanostructures, both concentric tubular composites, where an outer tubule of one material surrounds an inner tubule of another,[28] and segmented composite nanowires.[29,30] Segmented Co/Cu nanowires of this type have been used to study giant magnetoresistance in multilayer systems.[30]

One of our earliest applications of the template method was to prepare ensembles of microscopic[31,32] and nanoscopic[33,34] electrodes. Such electrodes are prepared by depositing noble metals within the pores of commercially available polymeric filtration membranes. Initially, we deposited the metal in the pores using electrochemical plating methods,[31] but we ultimately discovered that electroless plating allowed for more uniform metal deposition.[33] In the electroless method, metal deposition begins at the pore walls, creating, at short deposition time, hollow metal nanotubules within the pores.[8−12] That is, the electroless plating method yielded metal (typically gold) nanotubule membranes, the subject of this review.

Coincidentally, there is also a long-standing interest in our research group in the area of membrane-based chemical separations.[35−37] This interest led us to undertake a series of fundamental investigations of the transport properties of the gold nanotubule membranes. We discovered that by controlling the Au deposition time, we could prepare Au nanotubules that had effective (vide infra) inside diameters of molecular dimensions (<1 nm).[9] This suggested that these membranes might be useful as molecular sieves. In addition, because these membranes are composed of an electronically conductive material, it occurred to us that excess charge could be applied to the tubules by electrochemical charging in an electrolyte solution. We reasoned that it might be possible to use this excess charge to regulate ion transport across these membranes.[8] Finally, because the tubules are composed of gold, it seemed possible that we could use well-known Au-thiol chemistry to change the chemical environment within the tubules and, via this route, introduce chemical- and ion-transport selectivity into these membranes.[10−12]

Progress to date on using chemisorbed thiols to control the transport properties of the Au nanotubule membranes is reviewed here. We begin by briefly discussing the polycarbonate template membranes and the electroless deposition method used to prepare the Au nanotubules. The gas-transport method used to obtain the effective inside diameter of the tubules is also briefly reviewed. We then discuss the use of electrically neutral thiols to introduce chemical-transport selectivity in the Au nanotubule membranes. We conclude with a review of the use of electrically charged thiols to control ion-transport selectivity in these membranes.

10.1021/cm0101071 CCC: $20.00
Published on Web 07/03/2001

II. Membrane Preparation and Analysis

A. Template Membranes Used. Commercially available "track-etched" polycarbonate filters are used as the templates to prepare the Au nanotubules. The track-etch process[4] entails bombarding a solid material (in this case an approximately 10-μm-thick polycarbonate film) with a collimated beam of high-energy nuclear fission fragments to create parallel damage tracks in the film. The damage tracks are then etched into monodisperse cylindrical pores by exposing the film to an aqueous base. The diameter of the pores is determined by the etch time and the etch-solution temperature. The density of pores is determined by the exposure time to the fission-fragment beam. Membranes with pore diameters ranging from as small as 10 nm to as large as $\approx$10 μm are available commercially.

The membranes used for these studies had nominal pore diameters of 30 nm and contained 6×10^8 pores/cm^2 of membrane surface area. The nominal pore diameter (supplied by the manufacturer) is obtained from scanning electron microscopic images of the film surface. Microscopic investigations of template-synthesized nanostructures prepared within the pores of such membranes have shown that the diameter of the pore in the center of the membrane is larger than the diameter at the membrane surface, that is, that cigar-shaped pores are obtained.[14,17] It has been suggested that this pore geometry arises because the fission fragment that creates the damage track also generates secondary electrons, which contribute to the damage along the track.[14]

B. Electroless Plating. The electroless plating method used to deposit the Au nanotubules within the pores of these membranes has been described previously.[11,33] Briefly, the template membrane is first "sensitized" by immersion into a $SnCl_2$ solution, which results in deposition of Sn(II) onto all the membrane's surfaces (pore walls and membrane faces). The sensitized membrane is then immersed into a $AgNO_3$ solution, and a surface redox reaction occurs (eq 1), which yields nanoscopic metallic Ag particles on the membrane surfaces. (The subscripts "surf" and "aq" denote species

$$Sn(II)_{surf} + 2Ag(I)_{aq} \rightarrow Sn(IV)_{surf} + 2Ag(0)_{surf} \quad (1)$$

adsorbed to the membrane surfaces and species dissolved in solution, respectively.) The membrane is then immersed into a commercial gold plating solution (Oromerse SO Part B, Technic, Inc.), and a second surface redox reaction occurs, to yield nanoscopic Au nanoparticles on the surfaces (eq 2).

$$Au(I)_{aq} + Ag(0)_{surf} \rightarrow Au(0)_{surf} + Ag(I)_{aq} \quad (2)$$

These surface-bound Au nanoparticles are good autocatalysts for the reduction of Au(I) to Au(0) using formaldehyde as the reducing agent. As a result, Au deposition begins at the pore walls, and Au tubules are obtained within the pores.[8−12] In addition, the faces of the membrane become coated with thin Au films. These surface films do not, however, block the mouths of the nanotubules, and there are open nanoscopic channels running from one face of the membrane to the other.

C. Determination of the Nanotubule Effective Inside Diameter. We use a gas-transport method to obtain an estimate of the inside diameter of the template-synthesized Au nanotubules.[11] Briefly, the tubule-containing membrane is placed in a gas-permeation cell, and the upper and lower half-cells are evacuated. The upper half-cell is then pressurized, typically to 20 psig with H_2, and the pressure−time transient associated with leakage of H_2 through the tubules is measured using a pressure transducer in the lower half-cell. The pressure−time transient is converted to gas flux (Q, mol s^{-1}), which is related to the radius of the nanotubules (r, cm) via[11,38]

$$Q = 4/3(2\pi/MRT)^{1/2}(nr^3\Delta P/l) \quad (3)$$

where ΔP is the pressure difference across the membrane (dyn cm^{-2}), M is the molecular weight of the gas, R is the gas constant (erg K^{-1} mol^{-1}), n is the number of nanotubules in the membrane sample, l is the membrane thickness (cm), and T is the temperature (K). (Note that n was labeled incorrectly as nanotubules per cm^2 in our previous publication.[11])

In using eq 3 we assume (1) that we know the number of nanotubules (n) in the membrane sample, (2) that the nanotubules have a constant inside diameter down their entire length, and (3) that the mechanism of gas transport through the membrane is Knudsen diffusion in the nanotubules. We have discussed the validity of each of these assumptions in detail in a recent review.[39] For this reason, these issues will not be reviewed again here. The key points to make are as follows: (1) Nanotubules with the smallest inside diameters have bottlenecks at the membrane surfaces. Hence, the values reported by the gas-flux method must be regarded as effective inside diameters (EID). (2) At long plating times the gas-flux measurement reports nanotubule EIDs that are of molecular dimensions (<1 nm). (3) Such membranes can be used to cleanly separate small molecules on the basis of molecular size,[9] which is the ultimate proof that the nanotubule EID is, indeed, of molecular dimensions.

III. Using Noncharged Thiols To Introduce Chemical-Transport Selectivity

It is well-known that thiols spontaneously chemisorb to Au surfaces and that this process can be accomplished by simply immersing the Au into a solution of the thiol.[10−12,40] It occurred to us that by chemisorbing a thiol to the inner tubule walls, the chemical environment within the tubules could be altered, and this, in turn, would change the transport properties of the membrane. The thiols used for these studies included linear C_3, C_{10}, and C_{16} alkanethiols and the more hydrophilic thiol HS−C_2H_4−OH.

A. Mechanism of Transport in the Thiol-Modified Membranes. To explore the transport mechanism, nanotubule membranes with EID = 2.0 nm were modified with the C_3, C_{10}, or C_{16} thiol, and the flux of toluene across each membrane was measured. A dilute aqueous solution of toluene was used as the feed. The flux plots (Figure 1) show that the rate of toluene transport increases with carbon chain length of the thiol. This might seem counterintuitive because the largest C_{16}

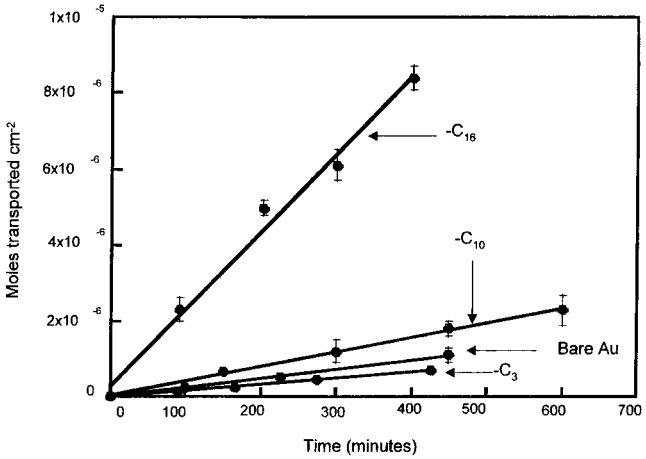

Figure 1. Flux plots for toluene in bare Au, and C_3, C_{10}, and C_{16} thiol modified nanotubule membranes; tubule EID = 2.0 nm.

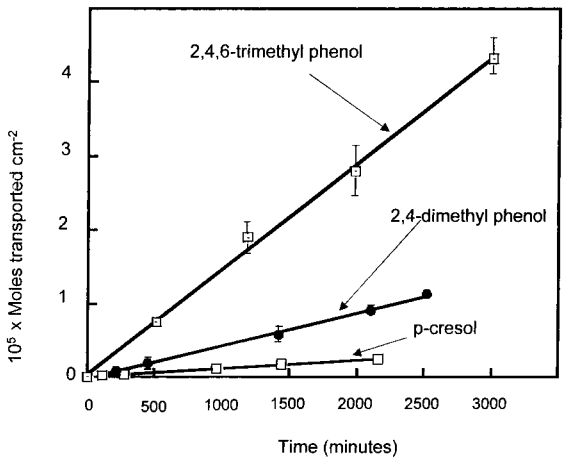

Figure 2. Flux plots for *p*-cresol, 2,4-dimethylphenol, and 2,4,6-trimethylphenol in an EID = 2.0 nm, C_{16}-derivatized Au nanotubule membrane.

chain might be expected to occlude the nanotubule, resulting in a lower effective diffusion coefficient for toluene in the membrane. However, the flux (J) is related to both the diffusion coefficient within the membrane (D) and the partition coefficient for the molecule between the aqueous feed solution and the membrane (K) (eq 4).[11] (C_{aq} is the concentration of the

$$J = -DKC_{aq}/l \qquad (4)$$

permeate molecule in the feed solution and l is the membrane thickness.)

Because D would be expected to decrease as the tubule becomes more occluded by the longer chain thiols, the data in Figure 1 suggest that the partition coefficient, K, increases with the chain length of the thiol employed. This is not surprising because analogous results were obtained from reversed-phase liquid chromatography experiments with alkyl silanes.[41] These data also show that any decrease in D due to possible occlusion of the nanotubule by the longest C_{16} thiol is more than offset by the increased partitioning term, K. We present below additional data that illustrate the importance of the partitioning term on transport in these membranes.

Gas-transport studies were used to further explore the issue of occlusion of the nanotubules by the C_{16} thiol.[11] The H_2 flux through a nanotubule membrane with tubule EID = 3.0 nm before chemisorption was remeasured after C_{16} thiol chemisorption. After chemisorption the tubule EID decreased to 2.0 nm, indicating that the thiol does, indeed, partially occlude the nanotubule. However, a decrease from 3.0 to 2.0 nm suggests that the thiol layers coating the inside walls of the Au nanotubules are on the order of 0.5 nm in thickness. The data of Porter et al. show that a well-formed and packed C_{16} monolayer should be ≈2.6-nm-thick.[40] This indicates that the monolayer on the inside tubule wall is neither well-ordered nor well-packed. Probing the nature of the monolayer within these nanoscopic tubules is an interesting and difficult scientific challenge.

While the gas-flux data show that the tubule is partially occluded by the C_{16} thiol, the effect this might have on the toluene diffusion coefficient depends on where within the membrane toluene is transported. There are two possibilities: transport occurs in the water-filled tubule that remains after chemisorption or transport occurs on or within the C_{16} phase itself. Ion-transport studies were used to explore this issue.[11] A C_{16}-modified membrane (2.0-nm EID tubules) was placed between a feed solution that contained $Ni(NO_3)_2$ and a permeate that was initially just water. The permeate was periodically assayed for Ni^{2+}, but no Ni^{2+} could be detected even after >40 h of permeation time. In contrast, Ni^{2+} was easily detected in the permeate when an unmodified (no thiol) membrane was used. These data show that because of the hydrophobicity of the C_{16} thiol, the tubules in this membrane are not wetted by water. Hence, transport of toluene occurs via the C_{16} phase within the tubules.

It is also of interest to explore the effect of hydrophobicity of the permeate molecule, within a homologous series, on flux in the C_{16}-modified membrane. Figure 2 shows flux plots for *p*-cresol, 2,4-dimethylphenol, and 2,4,6-trimethylphenol in a membrane that had EID = 2.0-nm tubules. The flux increases with increasing molecular weight for the members of this series. Again, this result is counterintuitive if only the diffusion coefficient for the permeate molecule in the membrane is considered. However, the partition coefficients for these molecules between the aqueous feed solution and the C_{16} phase would be expected to increase in the order *p*-cresol < 2,4-dimethylphenol < 2,4,6-trimethylphenol. Analogous to the data in Figure 1, the data in Figure 2 clearly show that transport in this membrane is dominated by the partition term in eq 4.

B. Hydrophobic/Hydrophilic Transport Selectivity—Single-Molecule Permeation Experiments. We wanted to explore the possibility of using the thiol-modified membranes to separate molecules based on their chemical properties. The most rudimentary example would be the separation of hydrophobic from hydrophilic molecules. Figure 3A compares flux plots for toluene in a membrane modified with the hydrophobic C_{16} thiol and a membrane modified with the hydrophilic C_2H_4OH thiol (3.0-nm EID tubules). The flux of toluene is 1 order of magnitude higher in the C_{16} membrane than in the C_2H_4OH membrane (Table 1). Given the discussion above, this preferential transport of toluene in the hydrophobic membrane is not surpris-

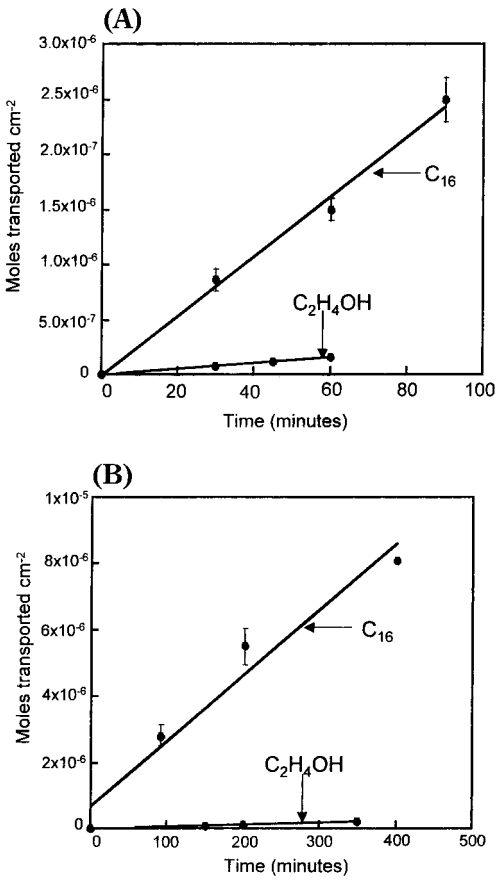

Figure 3. Flux plots comparing toluene transport in a C_{16} membrane and a $-C_2H_4OH$ membrane. Single-molecule permeation experiments. Nanotubule EID was (A) 3.0 nm and (B) 2.0 nm.

Table 1. Flux and Selectivity Data for Toluene in the C_{16} and C_2H_4OH Thiol Membranes[a]

membrane	nanotube diam (nm)	flux of toluene (mol cm^{-2} min^{-1})	α_{C_{16}/C_2H_4OH}
C_{16}	3.0	$(2.8 \pm 0.2) \times 10^{-8}$	
C_2H_4OH	3.0	$(2.6 \pm 0.4) \times 10^{-9}$	
			10
C_{16}	2.0	$(2.0 \pm 0.1) \times 10^{-8}$	
C_2H_4OH	2.0	$(6.1 \pm 0.4) \times 10^{-10}$	
			33

[a] Standard deviations are from replicate measurements on identical membranes.

ing. These data can be expressed in terms of a selectivity coefficient, α_{C_{16}/C_2H_4OH}, which is the flux of toluene in the C_{16} membrane divided by the flux in the C_2H_4OH membrane. For these EID = 3.0-nm nanotubule membranes $\alpha_{C_{16}/C_2H_4OH} = 10$ (Table 1).

Analogous toluene transport data were obtained for smaller EID = 2.0 nanotubule membranes (Figure 3B). Because of the smaller tubule diameter, the toluene fluxes in these membranes are lower than those in the EID = 3.0-nm membranes (Table 1). However, higher C_{16} vs C_2H_4OH selectivity ($\alpha_{C_{16}/C_2H_4OH} = 33$) is observed in the smaller EID nanotubule membranes. This increase in selectivity is largely due to the drop in flux of toluene in the C_2H_4OH membrane (Table 1). Because the partitioning advantage is diminished in this more hydrophilic membrane, flux is retarded by the smaller tubule EID.

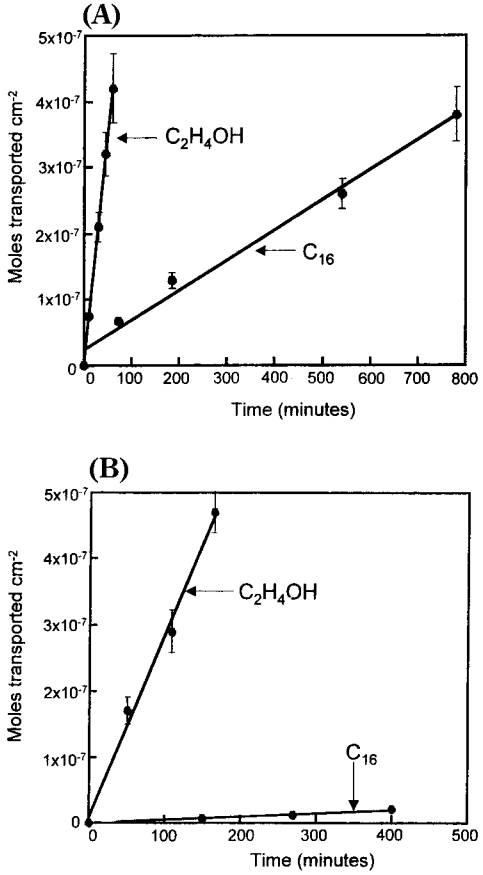

Figure 4. Flux plots comparing pyridine transport in a $-C_2H_4OH$ membrane and a C_{16} membrane. Single-molecule permeation experiments. Nanotubule EID was (A) 3.0 nm and (B) 2.0 nm.

Identical transport studies were done with the more hydrophilic permeate molecule pyridine.[11] Figure 4A shows the flux plots for the EID = 3.0-nm membranes treated with either the C_{16} or C_2H_4OH thiols. The selectivity pattern for the more hydrophilic pyridine is opposite that for the more hydrophobic toluene; that is, pyridine is preferentially transported in the C_2H_4OH membrane (Figure 4), whereas toluene is preferentially transported in the C_{16} membrane (Figure 3). This preferential transport of pyridine in the C_2H_4OH membrane can be quantified by defining a selectivity coefficient $\alpha_{C_2H_4OH/C_{16}}$, which is the flux of pyridine in the C_2H_4OH membrane divided by the flux in the C_{16} membrane. For these EID = 3.0-nm nanotubule membranes $\alpha_{C_2H_4OH/C_{16}} = 15$ (Table 2).

Figure 4B shows the analogous pyridine flux plots for the EID = 2.0 nanotubule membranes. Again, the flux of pyridine is higher in the C_2H_4OH membrane than in the C_{16} membrane. Furthermore, as was observed in the toluene transport studies (Table 1), the selectivity of pyridine transport is higher in the smaller EID = 2.0 nanotubule membranes ($\alpha_{C_2H_4OH/C_{16}} = 56$, Table 2). As noted above, the increased selectivity in the toluene case was largely due to decreased flux in the "nonpreferred" C_2H_4OH membrane. The same effect is observed in the pyridine case—the increased selectivity is largely due to the decreased flux in the "nonpreferred" C_{16} membrane. In this case the decreased flux is due to the thermodynamic penalty paid by the pyridine molecule

Table 2. Flux and Selectivity Data for Pyridine in the C_{16} and C_2H_4OH Thiol Membranes[a]

membrane	nanotube diam (nm)	flux of pyridine (mol cm^{-2} min^{-1})	$\alpha_{C_2H_4OH/C_{16}}$
C_2H_4OH	3.0	$(7.0 \pm 0.7) \times 10^{-9}$	
C_{16}	3.0	$(4.6 \pm 0.5) \times 10^{-10}$	
			15
C_2H_4OH	2.0	$(5.6 \pm 0.4) \times 10^{-9}$	
C_{16}	2.0	$(1.0 \pm 0.2) \times 10^{-10}$	
			56

[a] Standard deviations are from replicate measurements on identical membranes.

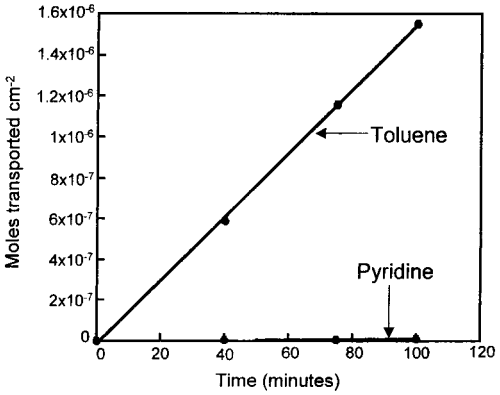

Figure 5. Flux plots showing toluene and pyridine transport in an EID = 2.0 nm, C_{16} nanotubule membrane. Two-molecule permeation experiment.

when it leaves the aqueous feed solution and enters the water-free tubules in the C_{16} membrane.[11]

C. Hydrophobic/Hydrophilic Transport Selectivity—Two-Molecule Permeation Experiments. The single-molecule permeation experiments suggest that the thiol-treated membranes can be used to separate hydrophobic species from hydrophilic species. To test this, two-molecule permeation experiments were conducted where the feed solution contained both pyridine and toluene. Figure 5 shows flux plots for toluene and pyridine from such a two-molecule experiment on a C_{16}-derivatized, EID = 2.0-nm nanotubule membrane.[11] The flux of toluene through this hydrophobic membrane is 165 times higher than the flux of pyridine. These data show that this membrane provides excellent selectivity for separation of hydrophobic from hydrophilic species.

IV. Using Ionizable Thiols To Control Ion-Transport Selectivity

A. A Chemisorbed Carboxylated Thiol. Ion-transport selectivity (also known as ion permselectivity) can be introduced into the Au nanotubule membranes by chemisorbing ionizable thiols.[12a,42,43] In a recent example, Hou et al. reported the use of chemisorbed HS-$(CH_2)_{10}$COOH to prepare pH-responsive membranes.[12a] They investigated the transport of benzene sulfonate (BS) across the membrane as a function of pH of the permeate and feed solutions. Figure 6 shows the variation of concentration of BS in the permeate half-cell (C_S) with diffusion time (t) measured at different solution pH values. The hydraulic radius of the nanotubules within this membrane was 8 nm.[12a] The initial concentration of BS in the feed half-cell in all cases was 1 mM. The flux of BS passing through the membrane was

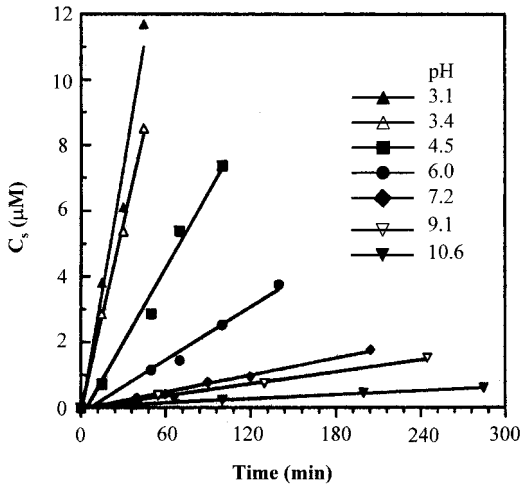

Figure 6. Diffusion of benzene sulfonate (BS) anions across a $HS(CH_2)_{10}COOH$ chemisorbed Au nanotubule membrane: effect of external pH. Used with permission from ref 12.

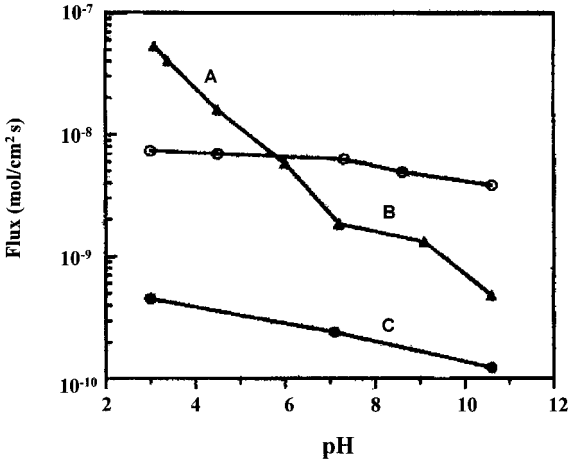

Figure 7. Flux of benzene sulfonate anion as a function of external pH obtained with (A) a $HS(CH_2)_{10}COOH$ chemisorbed Au nanotubule membrane, (B) a bare polycarbonate membrane, and (C) a Au nanotubule membrane, no thiol. Used with permission from ref 12.

determined from the slopes of the C_S-t plots shown in Figure 6 and these data are plotted in Figure 7 (curve A) as a function of the external pH. It is seen that the flux of BS decreases dramatically as the pH increases. Indeed, the flux of BS varies by a factor of 110 between pH 3.1 and 10.6. This change in flux with pH is about 10 times higher than that obtained with a pH-responsive poly(acrylic acid)—poly(ethylenimine) complex membrane described by Kono et al.[44]

The pH-dependent fluxes observed can be explained in terms of electrostatic interactions between the membrane and the anionic BS molecule. It is first important to point out that, at the ionic strength used in the feed and permeate half-cells (2 mM), the electrical double layer, as approximated by the Debye length, would be expected to be on the order of 7 nm in thickness.[12a] Hence, as discussed in detail in our prior work,[8] the solution within the nanotubules is in essence a double-layer solution. As a result, at high pH values, where the surface carboxylic acid groups are ionized (anionic), the anionic BS molecule is electrostatically rejected by the membrane. In contrast, at low pH values, the

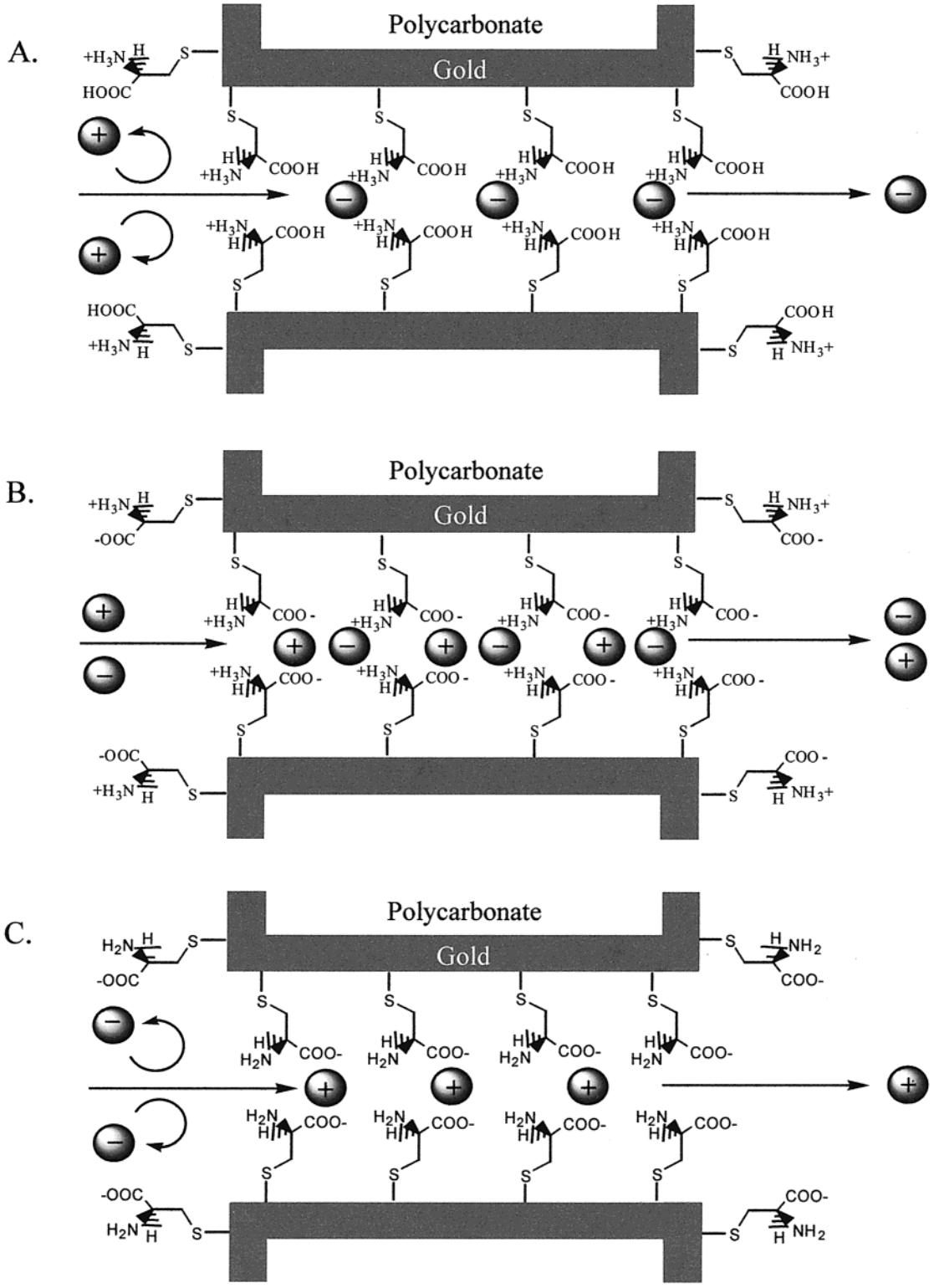

Figure 8. Schematic showing the three states of protonation and the resulting ion permselectivity of the chemisorbed cysteine. (A) Low pH, cation-rejecting/anion-transporting state. (B) pH = 6.0, non-ion-permselective state. (C) High pH, anion-rejecting/cation-transporting state. Note: ion transport in one direction (e.g., anions from left to right in (A)) is balanced by an equal flux of the same charge in the opposite direction so that electroneutrality is not violated in the two solution phases.

carboxylate groups are protonated and electrostatic rejection does not occur.

Curve B in Figure 7 shows the variation of BS flux with solution pH for the bare (no Au nanotubules) track-etched polycarbonate membrane. The flux changes by less than a factor of 2. Finally, curve C in Figure 7 shows that the fluxes of BS across a Au nanotubule membrane without the chemisorbed thiol are at least 15 times smaller than those obtained using the bare membrane at all pH values investigated. This result was attributed to the adsorption of Cl^- (present in the contacting solution phases), forming negative surface charge on the nanotubule walls. Recent studies have shown that BS anions can also adsorb to gold.[45] The variation of the

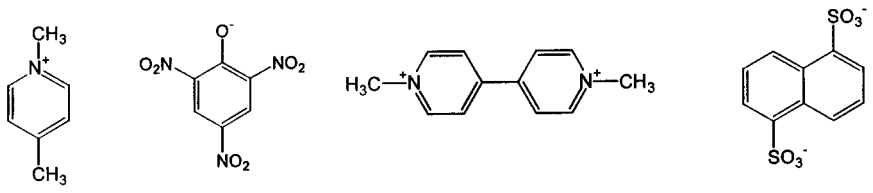

Figure 9. Chemical structures and molecular volumes for the permeate ions investigated here.

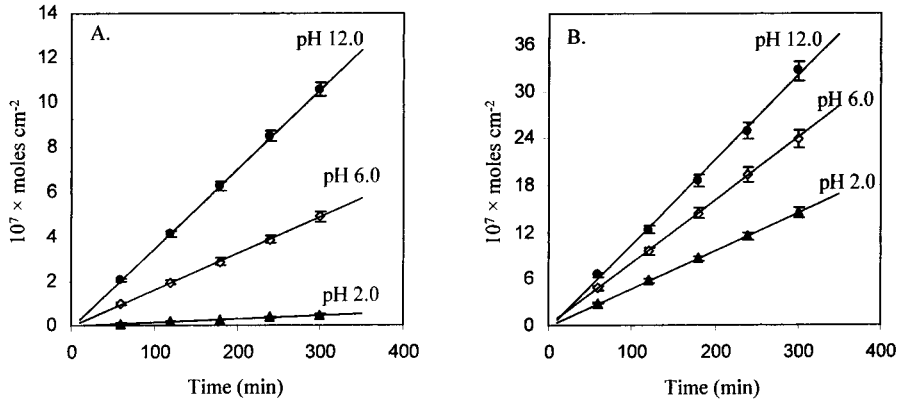

Figure 10. Permeation data for (A) MV^{2+} and (B) DMP^{+} at various pH values for the 1.4-nm-EID Au nanotubule membrane modified with L-cysteine. The error bars represent the maximum and minimum values obtained from three replicate measurements.

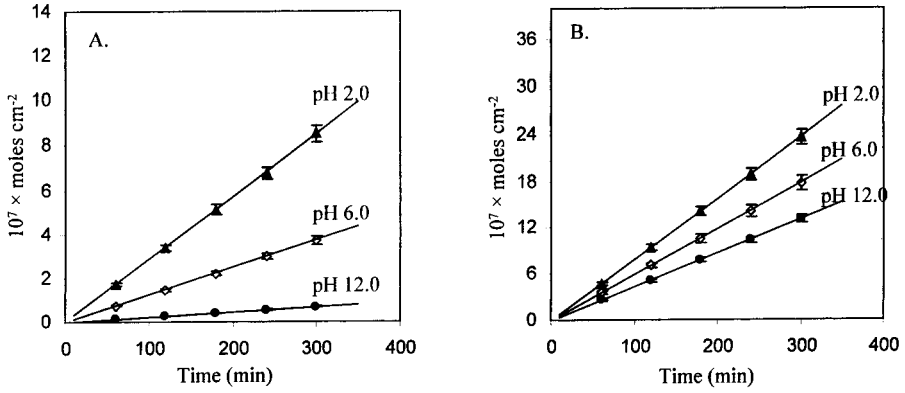

Figure 11. Permeation data for (A) NDS^{2-} and (B) Pic^{-} at various pH values for the 1.4-nm-EID Au nanotubule membrane modified with L-cysteine. Error bars as per Figure 10.

flux of BS shown in curve C is likely caused by pH-dependent dissociation of the adsorbed Cl^{-} or BS anions.[12a]

B. pH-Switchable Ion-Transport Selectivity in Membranes Based on Chemisorbed Cysteine. The unique feature of the chemisorbed amino acid is that depending on the solution pH value, the membrane can have excess positive charge (low pH, protonated amino group), no net charge (isoelectric point, protonated amino and deprotonated carboxyl), or excess negative charge (high pH, deprotonated carboxyl). As a result, these membranes can be switched between cation-transporting (anion-rejecting), non-ion-permselective, and anion-transporting (cation-rejecting) states (Figure 8).[43] The permeate ions used for these studies were methyl viologen (MV^{2+}), 1,5-naphthalene disulfonate (1,5-NDS^{2-}), 1,4-dimethylpyridinium (DMP^{+}), and picric acid (Pic^{-}) (Figure 9). The permeate half-cell initially contained only buffer solution at a pH of 2.0, 6.0, or 12.0. The feed half-cell was 10 mM in the ion of interest dissolved in the same buffer solution.

Figure 10 shows plots of moles of MV^{2+} and DMP^{+} transported vs time across a membrane with 1.4-nm-EID Au nanotubules as a function of pH of the contacting solution phases.[43] Figure 11 shows the analogous plots for the anionic permeates, 1,5-NDS^{2-} and Pic^{-}. As expected (Figure 8), the cationic permeates show high flux at pH = 12.0, low flux at pH = 2.0, and an intermediate flux value at pH = 6.0. The anionic permeates show the opposite trend—high flux at pH = 2.0 and low flux at pH = 12.0. The intermediate flux values obtained for both the anionic and the cationic permeates at pH = 6.0 indicates that this is near the isoelectric point of the chemisorbed cysteine.[43]

To quantify the variation in flux with pH, we define two selectivity coefficients: $\alpha_{pH2/pH12}$ for the anionic permeates and $\alpha_{pH12/pH2}$ for the cationic permeates:

$$\alpha_{pH2/pH12} = (\text{flux of anion at pH} = 2.0)/(\text{flux of anion at pH} = 12.0) \quad (5)$$

$$\alpha_{pH12/pH2} = (\text{flux of cation at pH} = 12.0)/(\text{flux of cation at pH} = 2.0) \quad (6)$$

These selectivity coefficients are defined such that the high flux value is divided by the low flux value to yield, in both cases, an α value greater than unity. Table 3 shows selectivity coefficient data for membranes containing Au nanotubules with four different EID values.

For the cationic permeates, the selectivity coefficient for the divalent MV^{2+} is always greater than that for the monovalent DMP^{+}. Because the selectivity is based on electrostatics (e.g., rejection of the cation by the protonated amino group at pH = 2.0, Figure 8A), this effect of magnitude of the permeate charge was anticipated. The same trend (higher selectivity coefficients for the divalent) is observed for the anionic permeates in the 1.4-nm-EID tubules. Interestingly, the selectivity coefficients for 1,5-NDS^{2-} and Pic^{-} are the same for the membrane containing the smallest EID tubules (Table 3). This is due to molecular sieving in these nanoscopic tubules, which discriminates against the larger 1,5-NDS^{2-}.[43] Finally, as would be expected, selectivity, in general, increases with decreasing nanotubule EID.

These single-ion-transport experiments suggest that these membranes might be useful for separating anionic and cationic species. To test this, we did a two-ion permeation experiment with the salt MV^{2+}1,5-NDS^{2-}.[43] Figure 12A shows absorption spectra for 1.0×10^{-5} M MV^{2+}, 1,5-NDS^{2-}, and MV^{2+}1,5-NDS^{2-}. 1,5-NDS^{2-} shows a characteristic sharp band centered at 225 nm where the MV^{2+} absorbance is very weak. MV^{2+} shows a strong band centered at 257 nm, where the 1,5-NDS^{2-} absorbance is weak.

Table 3. $\alpha_{pH12/pH2}$ and $\alpha_{pH2/pH12}$ Values

		selectivity coefficient	
permeate ion	nanotubule i.d. (nm)	$\alpha_{pH12/pH2}$	$\alpha_{pH2/pH12}$
DMP^{+}	0.9	6.4	
Pic^{-}	0.9		4.0
MV^{2+}	0.9	22	
NDS^{2-}	0.9		4.0
DMP^{+}	1.4	2.2	
Pic^{-}	1.4		1.8
MV^{2+}	1.4	24	
NDS^{2-}	1.4		12
MV^{2+}	1.9	10	
NDS^{2-}	1.9		6.8
MV^{2+}	3.0	6.9	
NDS^{2-}	3.0		5.9

Figure 12B shows the absorption spectrum for the permeate solution after 10 h of permeation at pH = 2.0 through a membrane with 1.4-nm-EID nanotubules. As would be expected, the absorption spectrum shows that, at this pH, the membrane preferential transports 1,5-NDS^{2-} and rejects MV^{2+}. From the known extinction coefficients and the measured absorbencies at 225 and 257 nm, the moles of both 1,5-NDS^{2-} and MV^{2+} transported into the permeate can be calculated. This calculation shows that the flux of 1,5-NDS^{2-} is 25 times higher than the MV^{2+} flux at pH = 2.0. This is in good agreement with the flux ratio value of 20 calculated from the slopes of the single-molecule permeation data (Figures 10 and 11).

Figure 12C shows the permeate absorption spectrum for an analogous transport experiment at pH = 12.0. Now the membrane is clearly anion-rejecting. The ratio of the MV^{2+} flux to 1,5-NDS^{2-} flux obtained from this spectrum is 110. This is almost 1 order of magnitude larger than the ratio of the fluxes calculated from the single-ion permeation data. This is a very interesting

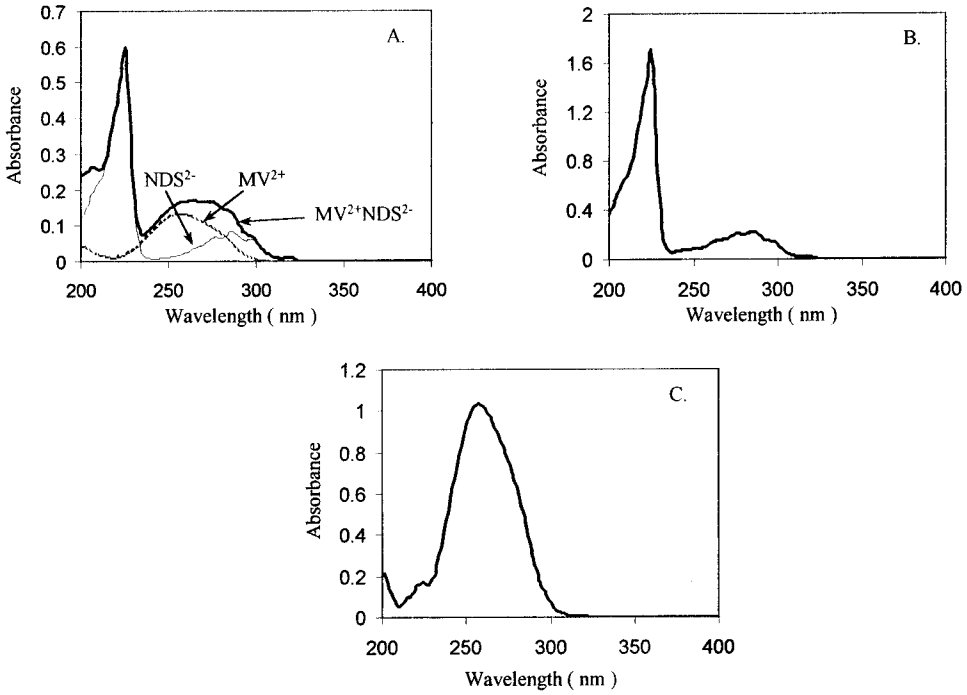

Figure 12. Absorption spectra for (A) 1.0×10^{-5} M MV^{2+}, NDS^{2-}, and $MV^{2+}NDS^{2-}$ salt and for permeate solution after 10-h permeation experiments at pH = (B) 2.0 and (C) 12.0. Nanotubule EID = 1.4 nm. The feed half-cell solution was 5 mM in the salt $MV^{2+}NDS^{2-}$.

result, which will require additional experimentation to fully interpret. Suffice it to say for now that at pH = 12 this membrane shows excellent separation of this anion/cation pair.

V. Conclusions

We have shown here that thiols can be used to introduce both chemical- and ion-transport selectivity in the Au nanotubule membranes. The use of cysteine is of particular interest because this allows for membranes that can be reversibly switched between anion-transporting/cation-rejecting and anion-rejecting/cation-transporting states. This ion permselectivity can be augmented by molecular-size-based transport selectivity. For example, a membrane in a cation-transporting state can discriminate between large and small cations because of the now well-documented molecular-sieving capabilities of these membranes.[9,43,46] It is important to add that while not reviewed here, we have also shown that ion-transport selectivity can be introduced and reversibly switched electrochemically as well.[8,46] When a potential that is negative of the potential of zero charge (pzc) is applied to the membrane, the nanotubules have excess negative charge, and the membrane rejects anions and transport cations. At applied potentials positive of the pzc, the nanotubules contain excess positive charge, and the membrane rejects cations and transport anions.[8]

We are pursuing possible applications of membranes of this type in chemical and bio-separations and sensors. For the chemical or bio-separations applications, flux or throughput across the membrane is an important issue. Flux is low for the membranes described here because the net porosity is low. We are currently attempting to make very high porosity metal or carbon nanotubule membranes for these applications. Flux is less of an issue in sensor applications. It is also important to note that because the nanotubule diameter, chemistry, and charge can be varied at will and completely independently of each other, these membranes are ideal model systems for fundamental investigation of how these parameters affect transport in membranes.

Finally, Mother Nature also makes nanotubules (e.g., protein[47] and ion channels[48]), and again she uses size, charge, and chemical interactions to determine what chemical species have access to these channels. The Au nanotubule membranes can also be viewed as model systems for these naturally occurring nanotubules. Furthermore, the Au nanotubules can perhaps be used to mimic transport in the natural channel systems. Such research at the bio/nano interface is of great current interest in our group.

Acknowledgment. Aspects of this work were funded by the National Science Foundation, the Office of Naval Research, and the Department of Energy.

References

(1) Martin, C. R. *Science* **1994**, *266*, 1961−1966.
(2) Hulteen, J. C.; Martin, C. R. *J. Mater. Chem.* **1997**, *7*, 1075−1087.
(3) Martin, C. R.; Mitchell, D. T. *Anal. Chem.* **1998**, *70*, 322A−327A.
(4) Fleischer, R. L.; Price, P. B.; Walker, R. M. *Nuclear Tracks in Solids*; University of California Press: Berkeley, CA, 1975.
(5) Hornyak, G L.; Patrissi, C. J.; Martin, C. R. *J. Phys. Chem. B* **1997**, *101*, 1548−1555.
(6) Possin, G. E. *Rev. Sci. Instrum.* **1970**, *41*, 772.
(7) Williams, W. D.; Giordano, N. *Rev. Sci. Instrum.* **1984**, *55*, 410.
(8) Nishizawa, M.; Menon, V. P.; Martin, C. R. *Science* **1995**, *268*, 700−702.
(9) Jirage, K. B.; Hulteen, J. C.; Martin, C. R. *Science* **1997**, *278*, 655−658.
(10) Hulteen, J. C.; Jirage, K. B.; Martin, C. R. *J. Am. Chem. Soc.* **1998**, *120*, 6603−6604.
(11) Jirage, K. B.; Hulteen, J. C.; Martin, C. R. *Anal. Chem.* **1999**, *71*, 4913−4918.
(12) Hou, Z.; Abbott, N. L.; Stroeve, P. *Langmuir* **2000**, *16*, 2401−2404. (b) Hou, Z.; Abbott, N. L.; Stroeve, P. *Langmuir* **1998**, *14*, 3287−3297.
(13) Tourillon, G.; Pontinnier, L.; Levy, J. P.; Langlais, V. Electrochem. *Solid-State Lett.* **2000**, *3*, 20−23.
(14) Schonenberger, C.; van der Zande, B. M. I.; Fokkink, L. G. J.; Henry, M.; Schmid, C.; Kruger, M.; Bachtold, A.; Huber, R.; Birk, H.; Staufer, U. *J. Phys. Chem. B* **1997**, *101*, 5497−5505.
(15) Preston, C. K.; Moskovits, M. J. *J. Phys. Chem.* **1993**, *97*, 8405.
(16) Martin, C. R. In *Handbook of Conducting Polymers*, 2nd ed.; Reynolds, J. R., Skotheim, T., Elsebaumer, R., Eds.; Marcel Dekker: New York, 1997; Chapter 16, pp 409−421.
(17) Duchet, J.; Legras, R.; Demoustier-Champagne, S. *Synth. Met.* **1998**, *98*, 113−122.
(18) Demoustier-Champagne, S.; Stavaux, P.-Y. *Chem. Mater.* **1999**, *11*, 829−834.
(19) Sukeerthi, S.; Contractor, Q. *Anal. Chem.* **1999**, *71*, 2231−2236.
(20) Lakshmi, B. B.; Patrissi, C. J.; Martin, C. R. *Chem. Mater.* **1997**, *9*, 2544−2550.
(21) Lakshmi, B. B.; Dorhout, P. K.; Martin, C. R. *Chem. Mater.* **1997**, *9*, 857−862.
(22) Che, G.; Lakshmi, B. B.; Martin, C. R.; Fisher, E. R. *Langmuir* **1999**, *15*, 750−758.
(23) Che, G.; Fisher, E. R.; Martin, C. R. *Nature* **1998**, *393*, 346−349.
(24) Kyotani, T.; Tsai, L. F.; Tomita, A. *Chem. Commun.* **1997**, 701.
(25) Patrissi, C. J.; Martin, C. R. *J. Electrochem. Soc.* **1999**, *146*, 3176−3180.
(26) Li, N.; Patrissi, C. J.; Martin, C. R. *J. Electrochem. Soc.* **2000**, *147*, 2044−2049.
(27) Che, G.; Jirage, K. B.; Fisher, E. R.; Martin, C. R.; Yoneyama, H., *J. Electrochem. Soc.* **1997**, *144*, 4296−4302.
(28) Cepak, V. M.; Hulteen, J. C.; Che, G.; Jirage, K. B.; Lakshmi, B. B.; Fisher, E. R.; Martin, C. R. *J. Mater. Res.* **1998**, *13*, 3070−3080.
(29) Martin, B. R.; Dermody, D. J.; Reiss, B. D.; Fang, M.; Lyon, L. A.; Natan, M. J.; Mallouk, T. E. *Adv. Mater.* **1999**, *11*, 1021−1025.
(30) Fert, A.; Piraux, L. *J. Magn. Magn. Mater.* **1999**, *200*, 338−358.
(31) Penner, R. M.; Martin, C. R. *Anal. Chem.* **1987**, *59*, 2625−2530.
(32) Cheng, I. F.; Martin, C. R. *Anal. Chem.* **1988**, *60*, 2163-2165.
(33) Menon, V. P.; Martin, C. R. *Anal. Chem.* **1995**, *67*, 1920−1928.
(34) Hulteen, J. C.; Menon, V. P.; Martin, C. R. *J. Chem. Soc., Faraday Trans. 1* **1996**, *92*, 4029−4032.
(35) Parthasarathy, R. V.; Menon, V. P.; Martin, C. R. *Chem. Mater.* **1997**, *9*, 560−566.
(36) Chen, W.-J.; Martin, C. R. *J. Membr. Sci.* **1995**, *104*, 101−108.
(37) Liu, C.; Martin, C. R. *Nature* **1991**, *352*, 50−52.
(38) Petzny, W. J.; Quinn, J. A. *Science* **1969**, *166*, 751
(39) Martin, C. R.; Nishizawa, M.; Jirage, K. B.; Kang, M. S. *J. Phys. Chem.*, in press.
(40) Porter, M. D.; Bright, T. B.; Allara, D. L.; Chidsey, C. E. D. *J. Am. Chem. Soc.* **1987**, *109*, 3559.
(41) Skoog, D. A.; Leary, J. J. *Principles of Instrumental Analysis*, 4th ed.; Saunders College Publishing: Orlando, FL, 1992.
(42) Jirage, K. B. Ph.D. Dissertation, Colorado State University, 1999; Chapter 4.
(43) Lee, S. B.; Martin, C. R. *Anal. Chem.*, in press.
(44) Kono, K.; Tabata, F.; Takagishi, T. *J. Membr. Sci.* **1993**, *76*, 233−43.
(45) Dutkiewicz, E.; Skoluda, P. *J. Chem. Soc., Faraday Trans.* **1996**, *92*, 3763−3767.
(46) Kang, M.; Martin, C. R. *Langmuir*, submitted for publication.
(47) Bayley, H. *Sci. Am.* **1997**, Sept, 62−67.
(48) Voet, D.; Voet, J. G. *Biochemistry*, 2nd ed.; Wiley: New York, 1995; pp 1297− 1298.

CM0101071